SMOKE PLUMES FROM CRUDE OIL BURNS

D. Evans, H.Baum, G. Mulholland, N. Bryner, G. Forney
U.S. National Institute of Standards and Technology
Gaithersburg, Maryland 20899

ABSTRACT

Measurements of optical properties and particle agglomeration of smoke from Alberta Sweet Blend Mix crude oil fires were made using a one cubic meter aging/dilution chamber. Measurements were made at ambient temperature simulating conditions in dilute smoke plumes away from the fire and at 100°C which simulates temperature conditions within several flame heights above the burning crude oil. Measurements of light transmission at three different wavelengths through the smoke collected in the chamber proved that the specific extinction coefficient of the carbonaceous agglomerate particles in the smoke is independent of the agglomerate size. These data are used as input to a calculation of smoke particle settling from the fire plume and deposition remote from the fire site. The calculation uses a large eddy simulation method to predict characteristics of wind blown buoyancy driven fire plumes. The calculation is capable of displaying the major features of smoke transport from the site of crude oil combustion. The process of smoke particulate settling from the plume is considered in detail by tracking representative smoke particles in the calculation. Results of example calculations are presented that demonstrate important features of the method.

BACKGROUND

In 1985, the Center for Fire Research (CFR) at the U.S. National Institute of Standards and Technology (NIST) began studies of oil spill combustion under support from the Minerals Management Service (MMS) of the U.S. Department of the Interior. This work seeks to quantify the processes involved in oil spill combustion on open waters and in water filled channels formed in broken ice including measurements of smoke production and prediction of smoke dispersal. Additional technical support from Environment Canada has allowed the study to be broadened in scope to include chemical analysis of the oil, oil residue, and oil smoke.

At the beginning of this research program it had already been demonstrated by other investigators that burning was an efficient means of removing crude oil from the surface of the water under a variety of conditions. Experimental burns of oil in ice leads (channels of water through ice) conducted by Brown and Goodman [1] and Smith and Diaz [2] showed that 50% to 90% of an oil spill could be removed by burning. In tests in which oil pools were free to spread during burning, Buist and Twardus [3] report consumptions of 70% to 90%. The focus of the research program at NIST was to quantify the combustion process and in particular measure properties of the smoke from the crude oil fires.

The goal of the NIST research program is to provide measurements and means to make quantitative predictions of (a) the fraction of oil in a spill

Environment Canada. Arctic and Marine Oil Spill Program Technical Seminar, 12th. June 7-9, 1989, Calgary, Canada, 1-22 pp, 1989.

that can be consumed by an in-situ combustion process, (b) the characteristics of the residual oil, and (c) the characteristics of the combustion product flow from the burning oil in the atmosphere. It is anticipated that this information may be cast into a form that is usable by local officials and oil spill response professionals as part of the decision making process in the event of an oil spill.

In the first year of the study [4], the burning process was studied at two pool diameters. 0.6 m and 1.2 m. The emission rate, size distribution, and specific extinction coefficient (relative blackness) were measured for the smoke produced by the fires. The structure of the smoke agglomerates was examined by electron microscopy. The burn residue left on the water by natural quenching of the combustion was analyzed and found to be depleted of short chain alkanes and cycloalkanes when compared with the fresh crude oil. A calculation of the induced air flow into a distribution of pool fires simulating the simultaneous burning of oil in many separate ice leads was performed to demonstrate the magnitude of the fire induced wind at ground level.

In the second year [5], extensive measurements of polynuclear aromatic hydrocarbon (PAH) content of the crude oil and the smoke were performed in close cooperation with Environment Canada. Measurements showed that about 10% of the crude oil was converted to smoke in the combustion process. A methodology was developed to predict the down wind dispersal of smoke generated by one or more oil spill fires in close proximity.

Last year [6], smoke emission was measured during the burning of oil layers thin enough to cause boiling in the supporting water layer. Under these conditions both smoke emission and the PAH content of the smoke was reduced compared to burning of thicker layers. Measurements of the optical properties and sedimentation velocities for aged and diluted smoke samples were performed. These characteristics are important in estimating smoke properties downwind of the oil spill fire. Analyses of smoke dispersal in the atmosphere were continued by formulating a model for smoke particle settling time which determines soot deposition on the ground remote from the combustion site.

This year measurements have focussed on the determination of the agglomeration rate for smoke particles at both ambient temperature conditions, which corresponds to the cooler, diluted smoke in the plume and at a temperature around 100°C, which corresponds to the temperature several flame heights above the fire. The plume dynamics model, that was started last year, is continued with a formulation in terms of buoyancy induced vortex trajectories (which represent the large scale plume turbulence) so that the agglomeration rate inferred from the laboratory measurements can be incorporated in the plume model. In the laboratory study, the agglomerate size increases with holding time in the aging/dilution collection chamber, while in a steady state plume model, the agglomerate size increases with downwind position along the plume, since downwind distance plays the role of time.

SMOKE AGING

As smoke rises in a plume from the burning oil, the smoke particles in the hot, fresh smoke collide and stick together forming larger particles. Downstream in the plume, changes also occur in the cooler, diluted smoke. As was shown in the 1986 report by Evans et al.[4], an individual smoke particle has a loose packed agglomerate structure made up of nearly spherical subunits with a typical diameter of about 50 nm. The colliding particles are actually agglomerates. Most particle growth studies have focussed on liquid droplets, which maintain a spherical shape after collisions, and these results are not applicable to agglomerate type structures. There is no data on the agglomeration rate for crude oil smoke.

Theoretical studies by Jones [7] and by Berry and Percival [8] lead to the conclusion that the spherical subunits in agglomerates absorb light as though they act independently of the agglomerate. This implies that the extinction coefficient per unit mass concentration of smoke is a constant independent of the agglomerate size, since light extinction is primarily a result of light absorption for carbonaceous particles. This prediction was tested by monitoring the specific extinction coefficient of smoke at three wavelengths as the smoke in the chamber agglomerates. The optical properties are required to calculate the absorption and scattering of solar radiation by the smoke.

The design of the aging/dilution facility was described in the 1988 Report by Evans et al. [5]. The key design features of the facility include rapid filling of the chamber in less than a minute, uniformly heated wall temperature up to 150°C, large volume (1 m^3) allowing aging for over an hour without significant wall loss, and a 100 liter piston allowing the volume of the chamber to be reduced as the smoke is extracted without the need of adding makeup air. The smoke collection system and the aging dilution system are illustrated in Figure 1.

The experiment consisted of burning Alberta Sweet crude oil floating on water in a 60 cm diameter pan. The smoke moving up the duct is mixed by a tripper plate and then is drawn isokinetically through a 10 cm sampling probe into the chamber. A fan continuously draws smoke through the chamber until the chamber is filled, then the two stainless steel butterfly valves, one on the inlet and one on the outlet, are simultaneously closed to capture a 1 m^3 sample. The smoke temperature in the stack is about 100°C, which is close to the chamber temperature for the high temperature aging experiments. In the case where the chamber is maintained at ambient conditions, it takes about 4 minutes for the gas to equilibrate to the wall temperature. A significant amount of cooling occurs as the gas is transported through the sampling line.

The number and mass concentration are monitored throughout the experiment. The mass concentration is monitored with a tapered-element oscillating microbalance (TEOM), which consists of a filter disk attached to the top of a hollow, oscillating tube. The mass concentration is determined from the flow rate through the tube and the change in the frequency of the tube oscillation as the smoke is deposited. This instrument allows continuous readout of smoke concentration. The number concentration is monitored by a

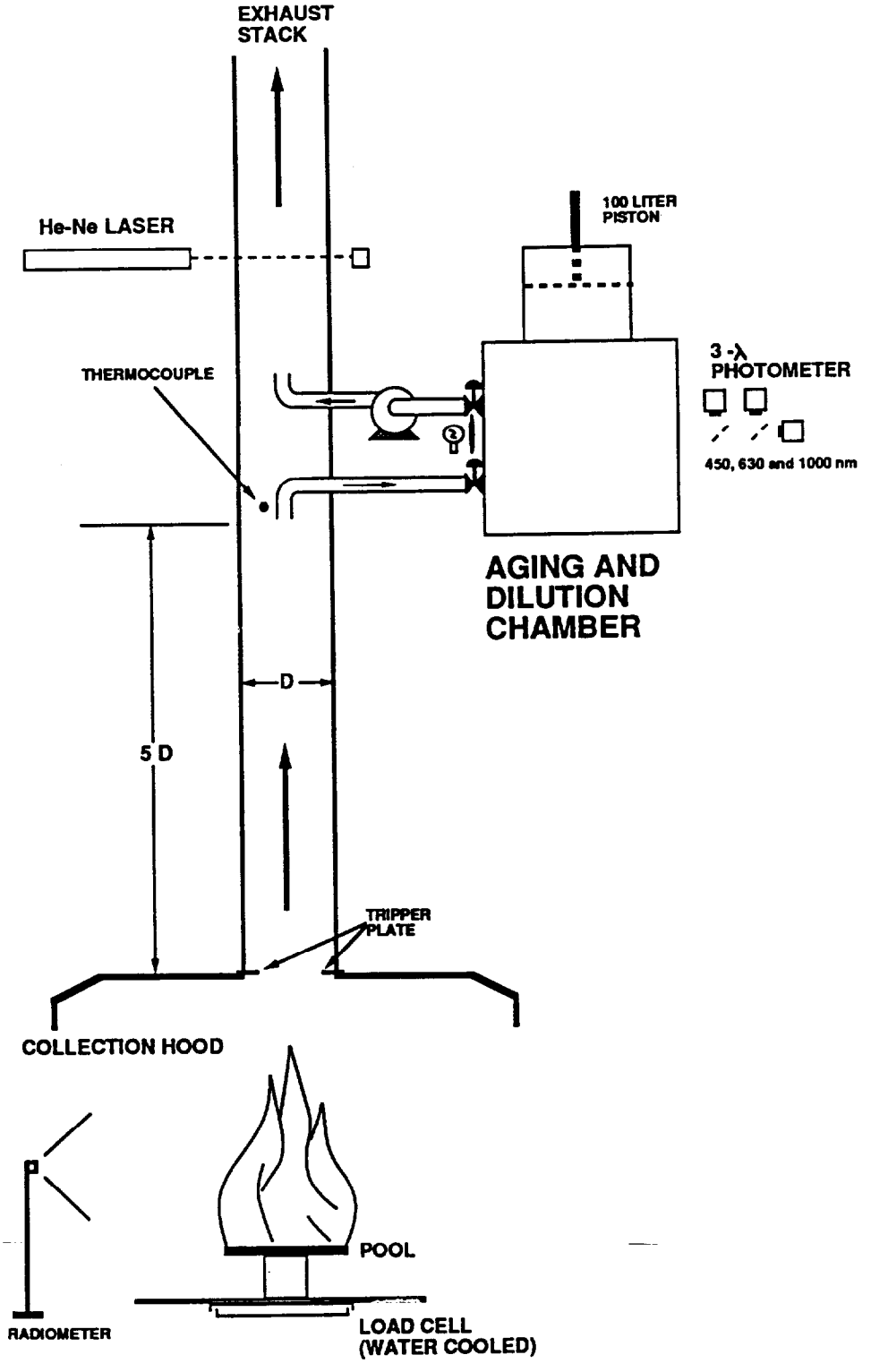

Figure 1. Schematic of the smoke collection system and aging dilution facility for crude oil burns.

continuous flow condensation nucleus counter (CNC), which utilizes butanol as the condensing vapor. The smoke is saturated with butanol as it flows above a reservoir of butanol heated to 30°C. Then the smoke flows through a cooled tube in which the vapor condenses on the smoke producing micrometer size butanol droplets. These droplets are counted optically by light scattering. The CNC gives a continuous readout of the number concentration of the smoke. The smoke is diluted by a factor of about 60 before entering the CNC to keep the concentration below 3.0×10^5 particles/cm^3, the saturation level of the instrument.

The number concentration begins at about 10^7 particles/cm^3 and decreases by a factor of about 50 over a 90 minute period as indicated in Figure 2. Most of this decrease is a result of particle agglomeration rather than wall loss, since over the same period of time the mass concentration decreased by a factor of two or less (Figure 3). The average mass of the agglomerate increases by about a factor of 30 as indicated in Figure 4. Assuming a primary particle size of 50 nm and a primary particle density of 2.0 g/cm^3, this change in mass corresponds to an increase in the number of primary units per agglomerate from about 200 at the initial time to a final value of about 6000.

The rate constant for agglomeration, Γ, is defined by the equation:

$$dN/dt = - \Gamma N^2, \tag{1}$$

where N is the number concentration of the agglomerates in terms of particle/cm^3. If Γ is assumed to be a constant, then equation (1) can be integrated to give

$$1/N - 1/N_0 = \Gamma t, \tag{2}$$

where N_0 is the initial number concentration. The plot of 1/N versus time in Figure 5 shows a linear behavior for times less than about 30 minutes. The curvature at later times is at least partly a result of particle loss to the walls becoming a significant factor at long times. Table 1 summarizes the experimental results for the agglomeration rate based on a linear least square fit of the data over the initial 10 to 20 minutes of each experiment. The values of Γ from repeat experiments differ by only a few percent; however, the uncertainty in the absolute value is large. We estimate the values of Γ to be $8 \pm 4 \times 10^{-10}$ cm^3/s for ambient conditions and $13 \pm 7 \times 10^{-10}$ cm^3/s for a temperature around 100°C. The sources of the uncertainty include the lack of an aerosol particle concentration standard, the reduced accuracy of the CNC from operation near saturation, and the use of a diluter. There is an additional uncertainty for the high temperature experiments resulting from thermophoretic particle losses as the warm smoke flows through the cool tube. The gas temperature drops from about 100°C to ambient conditions as the particles reach the CNC. The particle losses could be as large as 25%, which would reduce the agglomeration coefficient from about 13×10^{-10} cm^3/s to about 10×10^{-10} cm^3/s.

The light intensity transmitted through the aging dilution chamber was monitored at three wavelengths, 450, 630, and 1000 nm, using a photometer system designed by Cashdollar [9]. The specific extinction coefficient, σ,

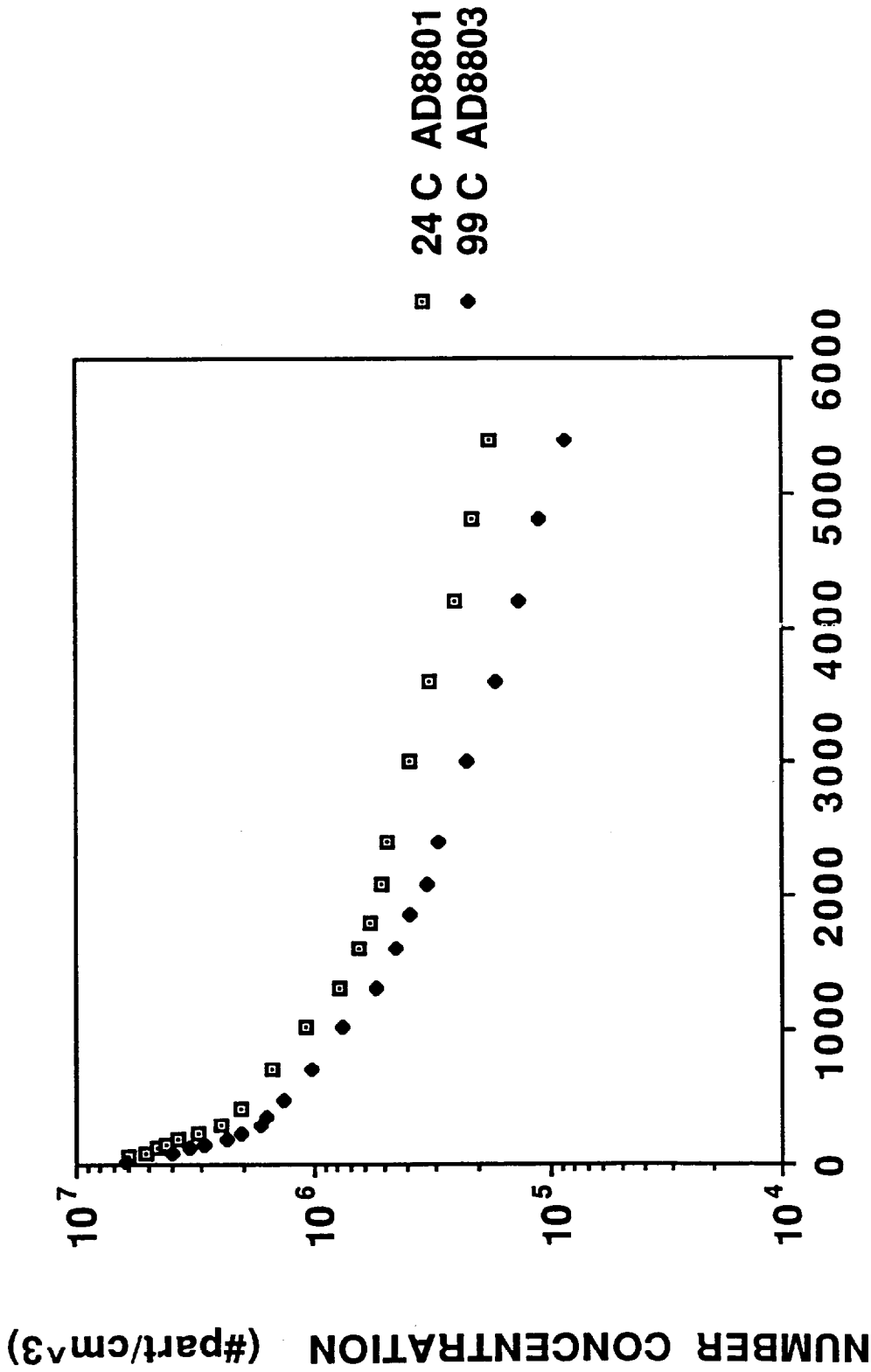

Figure 2. Number concentration versus time for aging of crude oil smoke at ambient and at elevated temperatures.

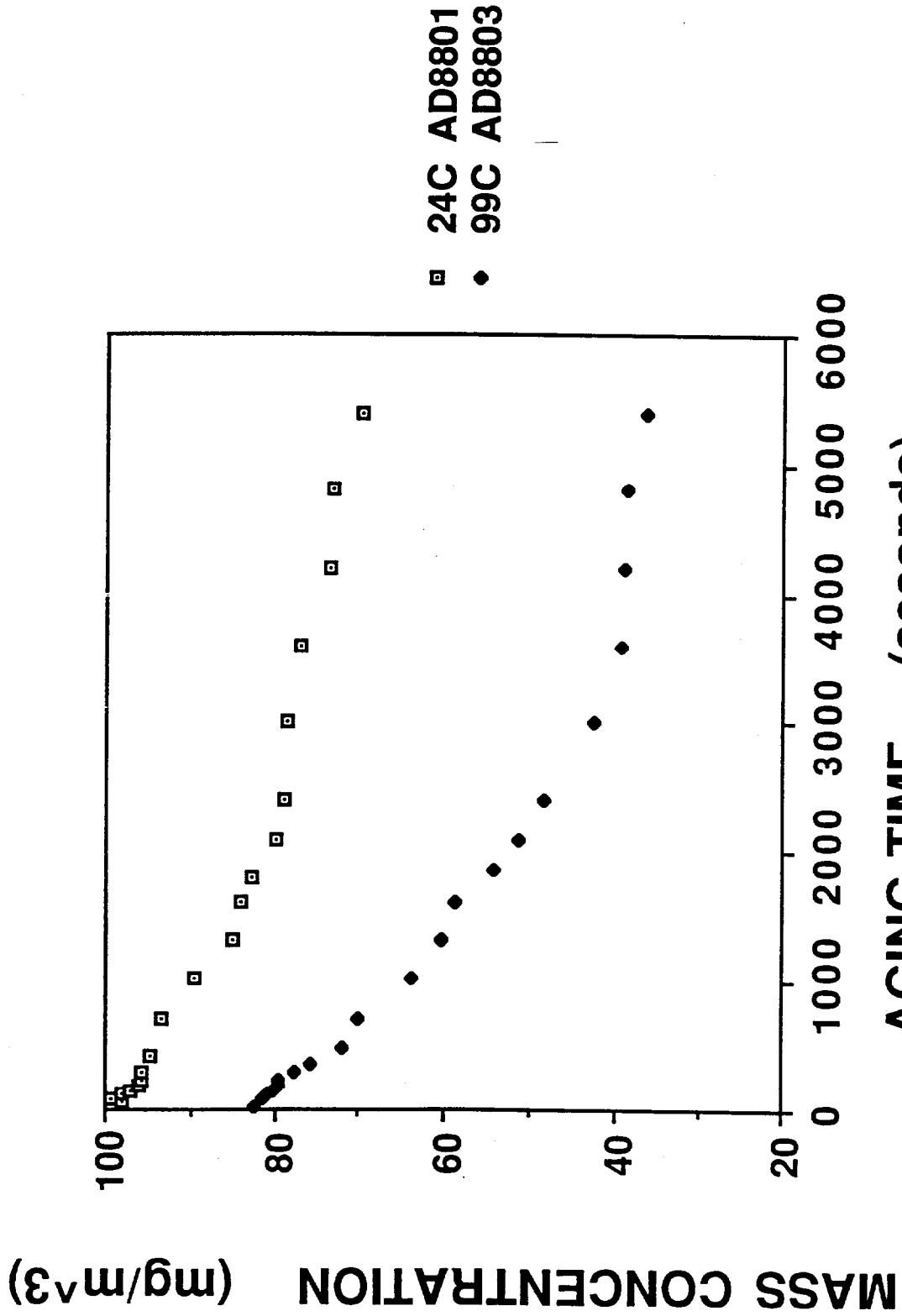

Figure 3. Mass concentration versus time for aging of crude oil smoke at ambient and at elevated temperatures.

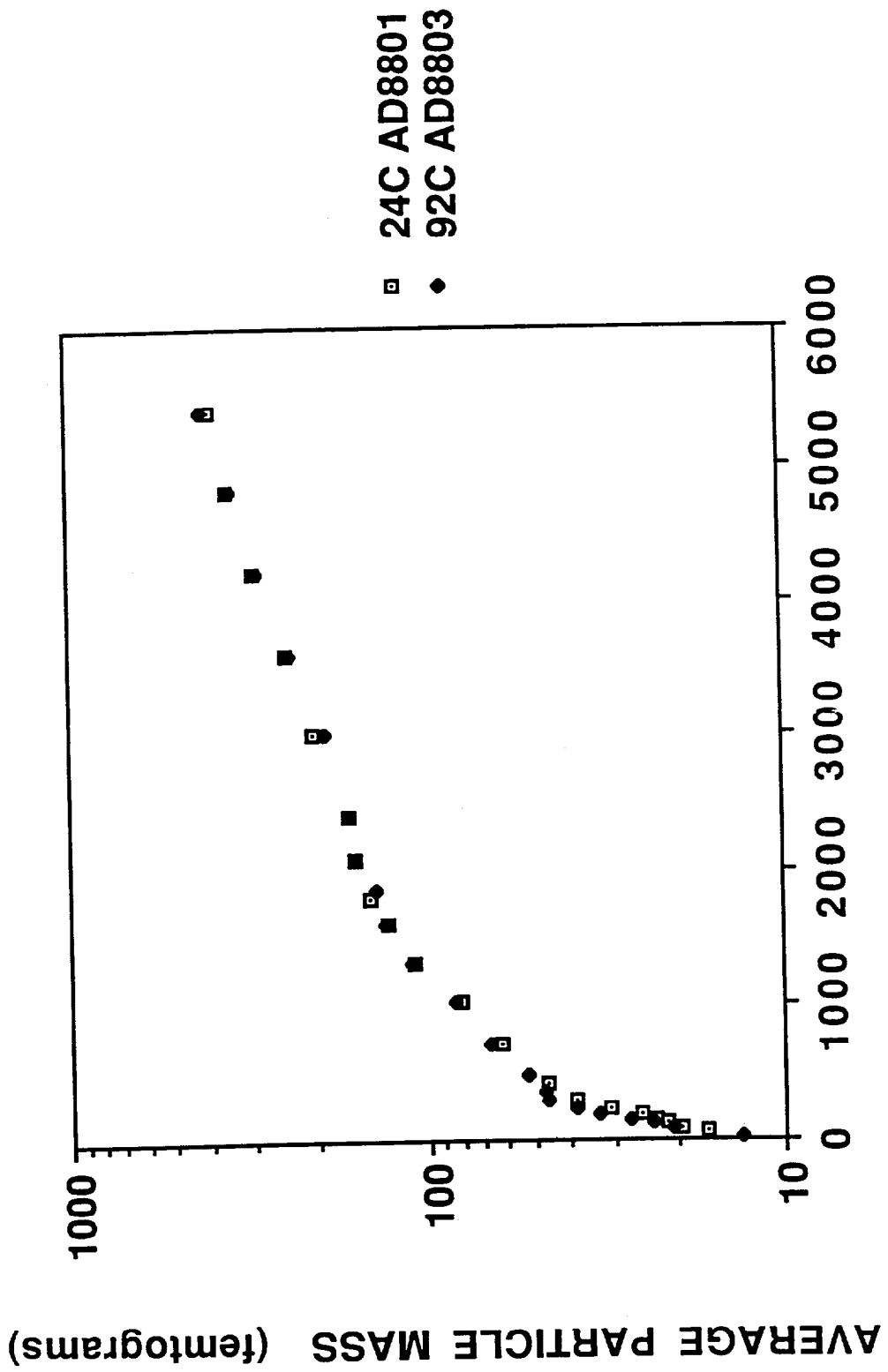

Figure 4. Average particle mass as a function of time for aging of crude oil smoke at ambient and at elevated temperatures.

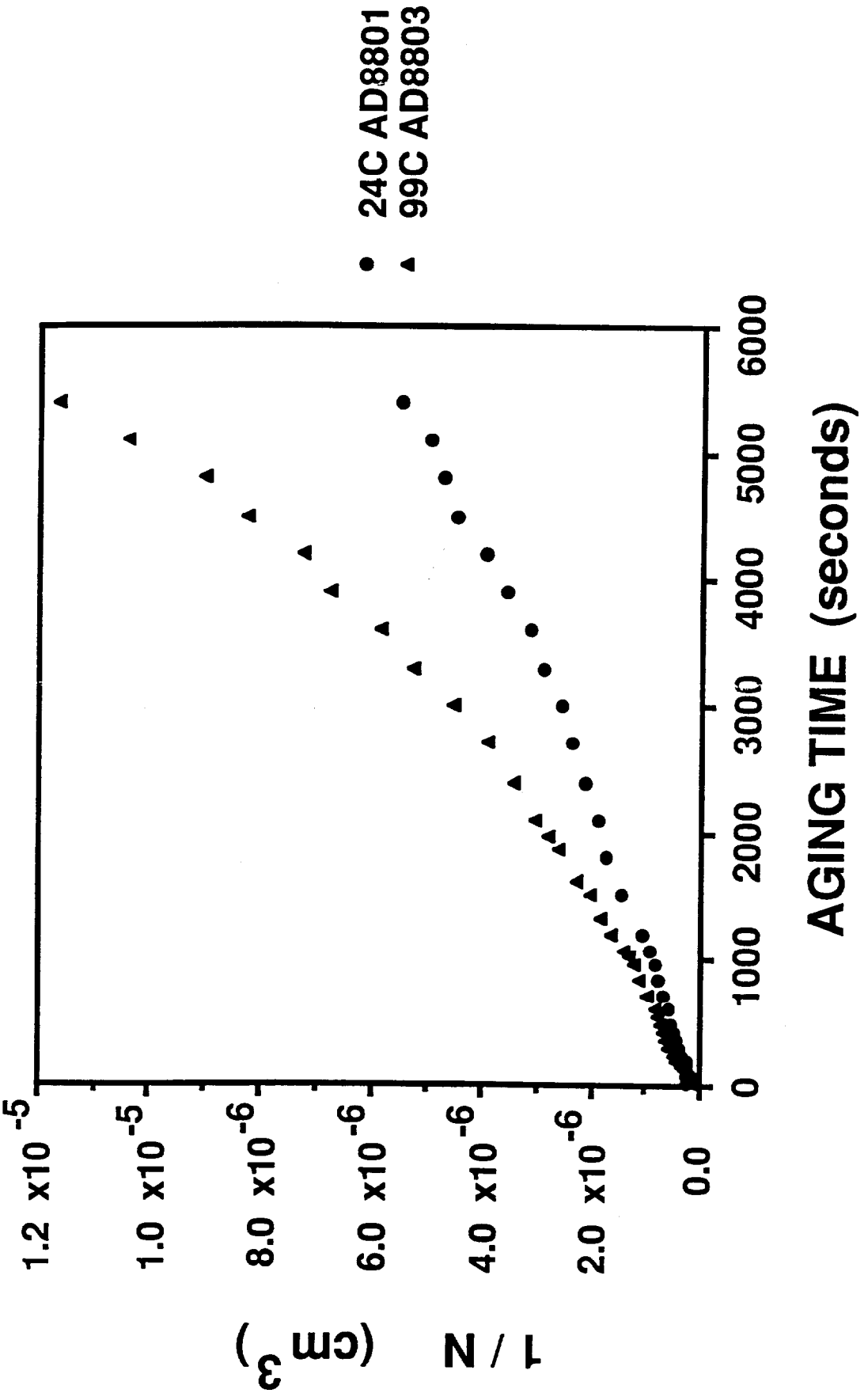

Figure 5. 1/Number Concentration versus time for aging of crude oil smoke at ambient and at elevated temperatures. The slope at small times is used for determining the coagulation coefficient.

Table I Agglomeration Rates For Smoke at Ambient Temperature and at Elevated Temperature

Run #	Temperature K	Fitting interval seconds	N_0 cm^{-3}	Γ cm^3/s
8801	297	60 - 720	6.0×10^6	7.9×10^{-10}
8805	297	30 - 1320	7.7×10^6	7.6×10^{-10}
8804	365	30 - 720	4.7×10^6	13.2×10^{-10}
8803	372	30 - 480	6.2×10^6	13.1×10^{-10}

Table II Average Values of Specific Extinction Cross-Section, σ

Run #	Temperature K	Time Interval seconds	$\sigma(450)$ m^2/g	$\sigma(630)$ m^2/g	$\sigma(1000)$ m^2/g
8801	297	30 - 5400	9.7	7.8	5.1
8805	297	30 - 5400	9.0	7.3	4.7
8804	365	30 - 5400	9.4	7.6	5.0
8803	372	30 - 4200	10.7	8.6	5.6
Avg. σ			9.7 ± 0.7	7.8 ± 0.6	5.1 ± 0.4

was obtained from the ratio of the extinction coefficient to the mass concentration of smoke as monitored by the TEOM. The value of σ did not change significantly over a 90 minute aging period for either the ambient temperature smoke or the hot smoke as shown in Figure 6. There was not a significant effect of the temperature of the smoke on the value of σ as shown in Table II. The results for σ for the four experiments are 5.1 ± 0.4 m^2/g (1000 nm), 7.8 ± 0.6 m^2/g (630 nm), and 9.7 ± 0.7 m^2/g (450 nm). These results are similar to the preliminary results presented in last years report by Evans et al. [5]. The variability in the TEOM performance is thought to be the main cause of the experimental uncertainty. This is supported by the observation that the variation in the ratio of the transmitted intensities for two wavelengths is less than 2% for all four tests. That is, the experimental variability is not caused by test to test variability in the smoke properties, but rather variability in the TEOM performance.

DISCUSSION OF SMOKE AGING

Mountain et al.[10] and Mulholland et al.[11] report computer simulations of the smoke agglomeration rate for the limiting cases of free molecular dynamics, in which the particle size is small compared to the mean free path of the gas, and continuum flow, in which the particle size is large compared to the mean free path of the gas. The experimental conditions approach continuum flow in terms of the agglomerate size, though there could still be a non-continuum effect arising from the primary particle size being smaller than the gas mean free path. The experimentally observed linear dependence of 1/(number concentration) on time is consistent with the continuum flow prediction; whereas, the free molecular flow leads to a quadratic dependence on time. The model predictions for the agglomeration rate for clusters composed of 200 primary units is based on a primary sphere size of 50 nm. The free molecular model leads to Γ equal to 3.0×10^{-8} cm^3/s at 300 K and 3.3×10^{-8} cm^3/s at 370 K. The continuum result for ambient conditions for an average cluster size of 12 is 6.0×10^{-10} cm^3/s, which is twice the coagulation coefficient of coalescing droplets. The continuum result for relatively small clusters is about 25% less than the observed result for much larger clusters and the free molecular result is about a factor of 40 higher than the measured result.

The predicted temperature dependence of Γ is approximately $(T)^{\frac{1}{2}}$ for both the free molecular and continuum flow condition. The temperature dependence inferred from the experiments is $(T)^{2.4}$. As discussed above, the experimental results for Γ at elevated temperatures are thought to be overestimates as a result of thermophoretic losses in the sampling lines.

PARTICULATE SETTLING ANALYSIS

The purpose of this section is to develop a method for solving the equations which govern the evolution of a smoke particle plume; from the point at which it is injected into the atmosphere until it is finally deposited on the ground. The principal assumptions underlying the model are:

1) The fire generating the smoke and hot gases is burning steadily.

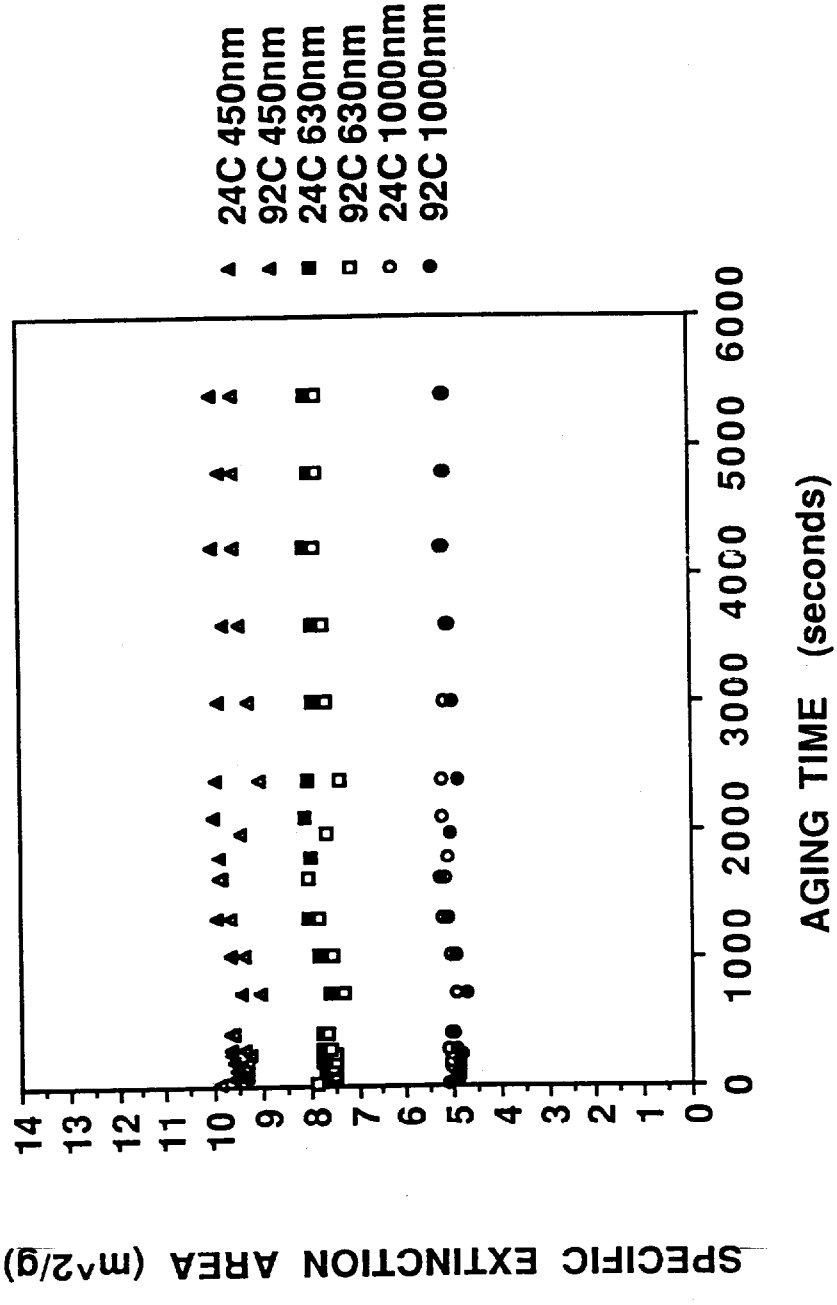

Figure 6. The specific extinction coefficient, σ, for 450 nm, 630 nm, and 1000 nm versus time for aging of crude oil smoke at ambient and at elevated temperatures.

2) The injection altitude and particle mass flux associated with the fire are known.

3) The gas temperature in the buoyant plume equilibrates with the atmosphere before any significant particle settling begins.

4) The ambient wind speed is much larger than the velocities induced by the negatively buoyant smoke particle plume.

5) Individual particle settling velocities are much smaller than the collective effects represented by the smoke particle plume.

6) The stratification of the atmosphere plays no role in the settling process.

The last assumption limits the injection altitude for which the analysis is valid to at most one kilometer. The determination of the injection altitude itself is not part of this analysis, although it does fit within the framework of the general approach. The goal of the present study is the ability to predict the downwind deposition pattern of the smoke particulate at ground level. The controlling parameters are the injection altitude and initial cross-section area of the plume, the particulate mass flux, and the ambient wind velocity.

To proceed, a cartesian coordinate system X,Y,Z is introduced as shown in figure 7. The variable X increases in the direction of the ambient wind, Z is directed vertically upward, and Y is horizontal coordinate perpendicular to the other two. Let U,V and W be the air velocity components in the X,Y and Z directions respectively. In this model U is the ambient wind speed and is presumed known. The smoke particulate is described in terms of a mass density ρ_p, mass flux M, and initial cross sectional area L^2. The initial injection altitude H is defined as the distance from the ground level to the initial center of mass of the plume. The atmosphere is characterized by an ambient density ρ_o and the magnitude of the gravitational acceleration is g. Dimensionless coordinates, velocity components, and smoke density can be introduced in terms of these parameters as follows:

$$\begin{aligned} (Y,Z) &= L\,(y,z) \\ X &= (LU)^{3/2}/(gM/\rho_o)^{1/2}t \\ (V,W) &= \{gM/(\rho_o UL)\}^{1/2}(v,w) \\ \rho_p &= M/(UL^2)\rho \end{aligned} \tag{3}$$

The dimensionless horizontal (v) and vertical (w) velocities induced by the settling process, as well as the dimensionless smoke particulate density ρ are functions of the reduced transverse horizontal coordinate (y), vertical coordinate (z), and downwind coordinate (t). This nomenclature is introduced because the mathematical model of this three-dimensional steady state process is equivalent to a two dimensional time dependent process viewed in a cross-sectional plane moving downwind at the ambient wind speed U. Thus, the smoke distribution in the upwind plane $X=X_1$ in figure 7 evolves over a time interval defined by the second of eqs. (3) into the distribution at the downwind station $X=X_2$ in the figure.

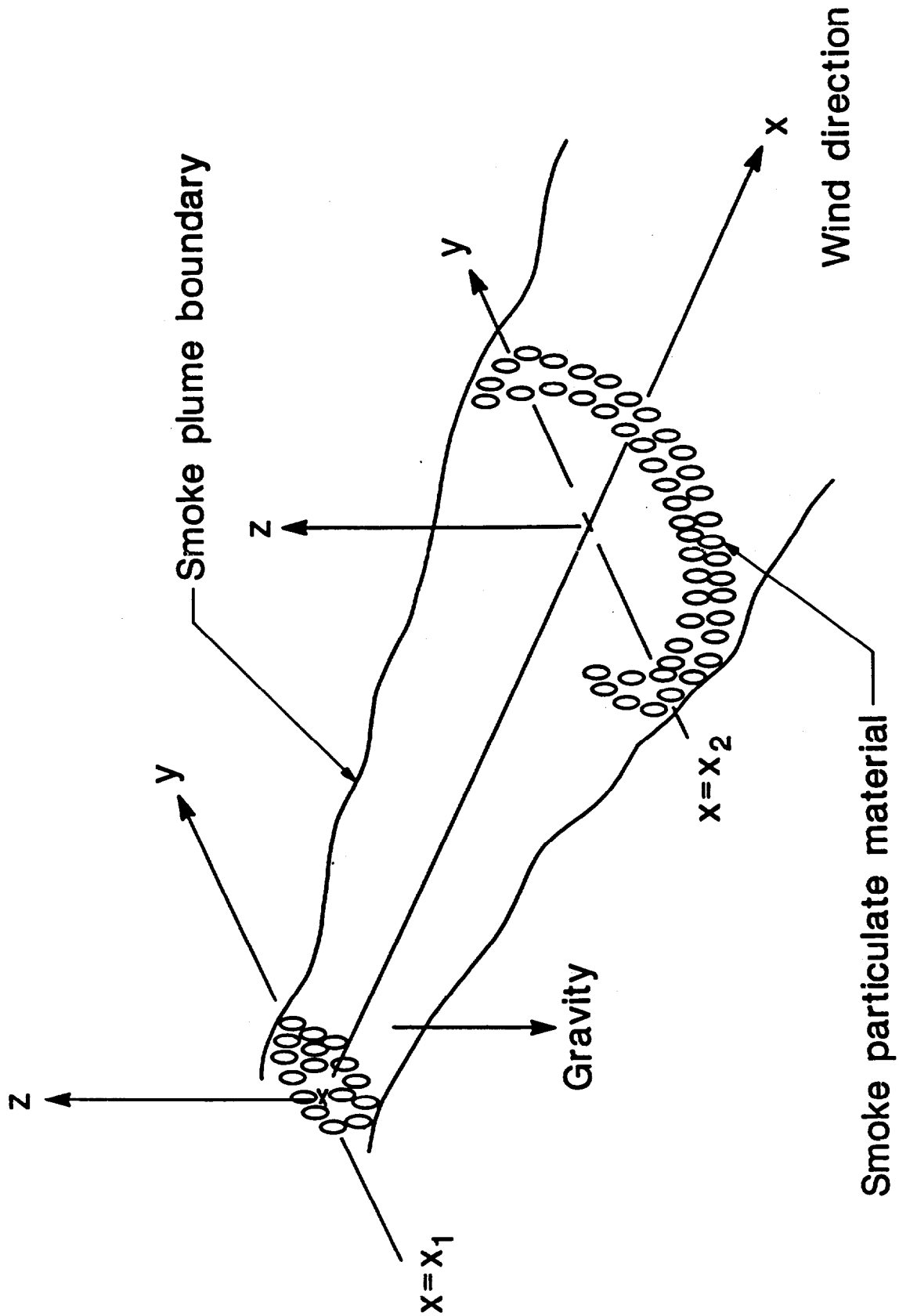

Figure 7. Schematic showing downwind evolution of smoke plume.

It is necessary to follow the particle density downwind until most of the smoke is within some specified small distance of the ground, at which point it can be regarded as having settled out of the system. Since the primary interest is in the location of the smoke particulate matter, the numerical method must focus on the Lagrangian coordinates of the smoke, rather than the general flow field. To this end, it is convenient to replace the continuous model of the smoke density by discrete clumps of matter as shown in figure 8. Each clump of matter carries a specific particulate mass flux and a vorticity which changes with time. The vorticity is induced by horizontal density gradients, with positive gradients inducing negative vorticity as illustrated in figure 8.

The mathematical basis for this discretization is the introduction of a Lagrangian coordinate system. Each clump of matter is characterized by its initial coordinates as follows:

$$\text{at} \quad t = 0; \; y = y_o; \; z = z_o$$

Then, the coordinates y, z of each clump are calculated as functions of time as solutions of the differential equations

$$\frac{\partial y}{\partial t} = v(y,z,t) \qquad \frac{\partial z}{\partial t} = w(y,z,t) \tag{4}$$

There is one pair of such equations for each clump; i.e. for each value of y_o, z_o. To generate the velocity fields, the evolution equations for the vorticity (the local angular velocity in the atmosphere)and density, need to be rewritten in terms of the new coordinate system. The appropriate formulae are:

$$\rho = f(y_o, z_o) \tag{5}$$

$$\frac{\partial \omega}{\partial t} = S\frac{\partial f}{\partial z_o} - T\frac{\partial f}{\partial y_o}$$

Here, the quantity ω is the vorticity while $f(y_o, z_o)$ is the initial upwind density distribution, and the density does not change in this system of coordinates. This is the mathematical statement of the fact that the mass flux associated with each clump is always the same as the clump progresses downwind.

The generation of the vorticity fields involves four coordinate gradients which describe the mixing and stretching of the fluid by the vortices. These quantities, denoted Q,R,S, and T are defined as follows:

$$\frac{\partial y}{\partial y_o} \equiv Q(y_o, z_o, t) \qquad \frac{\partial y}{\partial z_o} \equiv R(y_o, z_o, t) \tag{6}$$

$$\frac{\partial z}{\partial y_o} \equiv S(y_o, z_o, t) \qquad \frac{\partial z}{\partial z_o} \equiv T(y_o, z_o, t)$$

To preserve the accuracy of this method, it is important not to actually compute any spatial derivatives numerically. To avoid this, we note that <u>analytical</u> recipes for v(y,z,t) and w(y,z,t) can be generated and that these

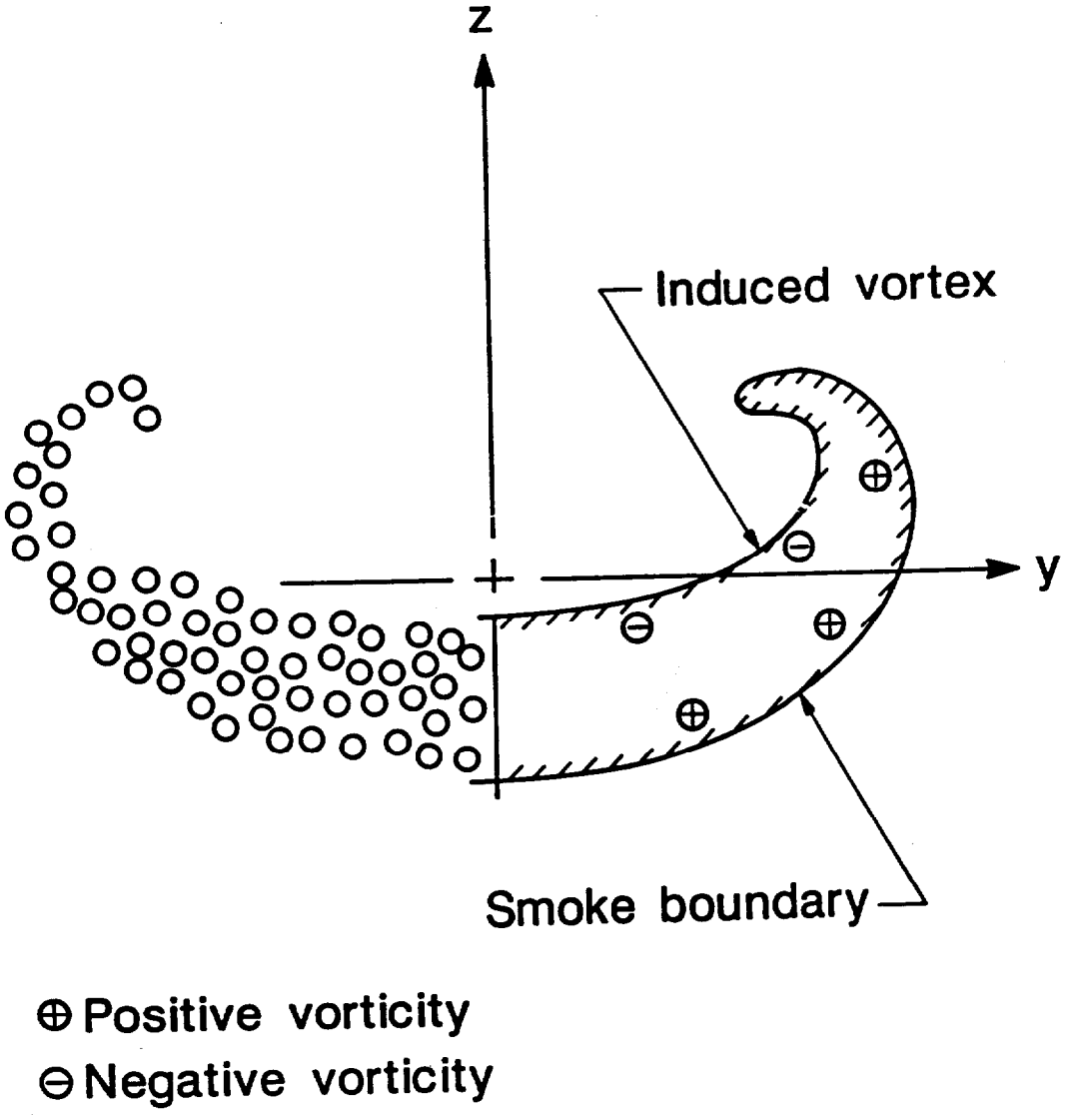

Figure 8. Discretization of smoke into vorticity containing clumps. Horizontal density gradients induced vorticity.

recipes can be exactly differentiated. The procedure for generating these recipes will be indicated briefly below. Given the existence of such expressions, however, it is easy to generate evolution equations for Q,R,S, and T. The necessary equations are:

$$\frac{\partial Q}{\partial t} = Q \frac{\partial v}{\partial y} + S \frac{\partial v}{\partial z}$$

$$\frac{\partial R}{\partial t} = R \frac{\partial v}{\partial y} + T \frac{\partial v}{\partial z} \qquad (7)$$

$$\frac{\partial S}{\partial t} = Q \frac{\partial w}{\partial y} + S \frac{\partial w}{\partial z}$$

$$\frac{\partial T}{\partial t} = R \frac{\partial w}{\partial y} + T \frac{\partial w}{\partial z}$$

Equations (4), (5), and (7) constitute a set of seven ordinary differential equations and one algebraic statement that must be solved to describe the evolution of each clump. They are equivalent to solving the equations of fluid motion everywhere in space. Obviously, any method which attempts to solve the equations everywhere is going to yield a much cruder approximation to the quantities of interest than one which concentrates attention directly on the area occupied by smoke. Thus, it is worthwhile to expend this much effort on tracking the fate of a single clump of particulate matter, if no resources have to be devoted to calculating quantities outside the smoke cloud.

The final piece of information required to implement this method is the explicit representation of the velocities in terms of the coordinates y,z. To this end, it is convenient to introduce a stream function $\Psi(y,z,t)$ that is related to the velocities by:

$$\frac{\partial \Psi}{\partial z} = v; \quad \frac{\partial \Psi}{\partial y} = - w \qquad (8)$$

The requirement that the velocity fields conserve mass yields an equation for Ψ in terms of ω. The solution can be expressed in terms of a Greens function $G(y,z,y_o,z_o)$ as:

$$\Psi = \iint dy_o dz_o \; G(y,z,y_o z_o) \; \omega(y_o, z_o t)$$

$$G = \frac{1}{2\pi} \left\{ \log (r_+) - \log (r_-) - \log (rI_-) + \log (rI_+) \right\}$$

$$(r_+)^2 = (y-y_o)^2 + (z-z_o)^2$$

$$(r_-)^2 = (y+y_o)^2 + (z-z_o)^2 \qquad (9)$$

$$(rI_-)^2 = (y-y_o)^2 + \{z + [2(H/L) + z_o]\}^2$$

$$(rI_+)^2 = (y+y_o)^2 + \{z + [2(H/L) + z_o]\}^2$$

Physically, the Greens function represents the flow induced by the vortex pair associated with two clumps as shown in figure 9a. The signs of the vortices are such that the direction of the swirling motion, as indicated by the arrows, induces a downward flow. This accounts for the first two terms in

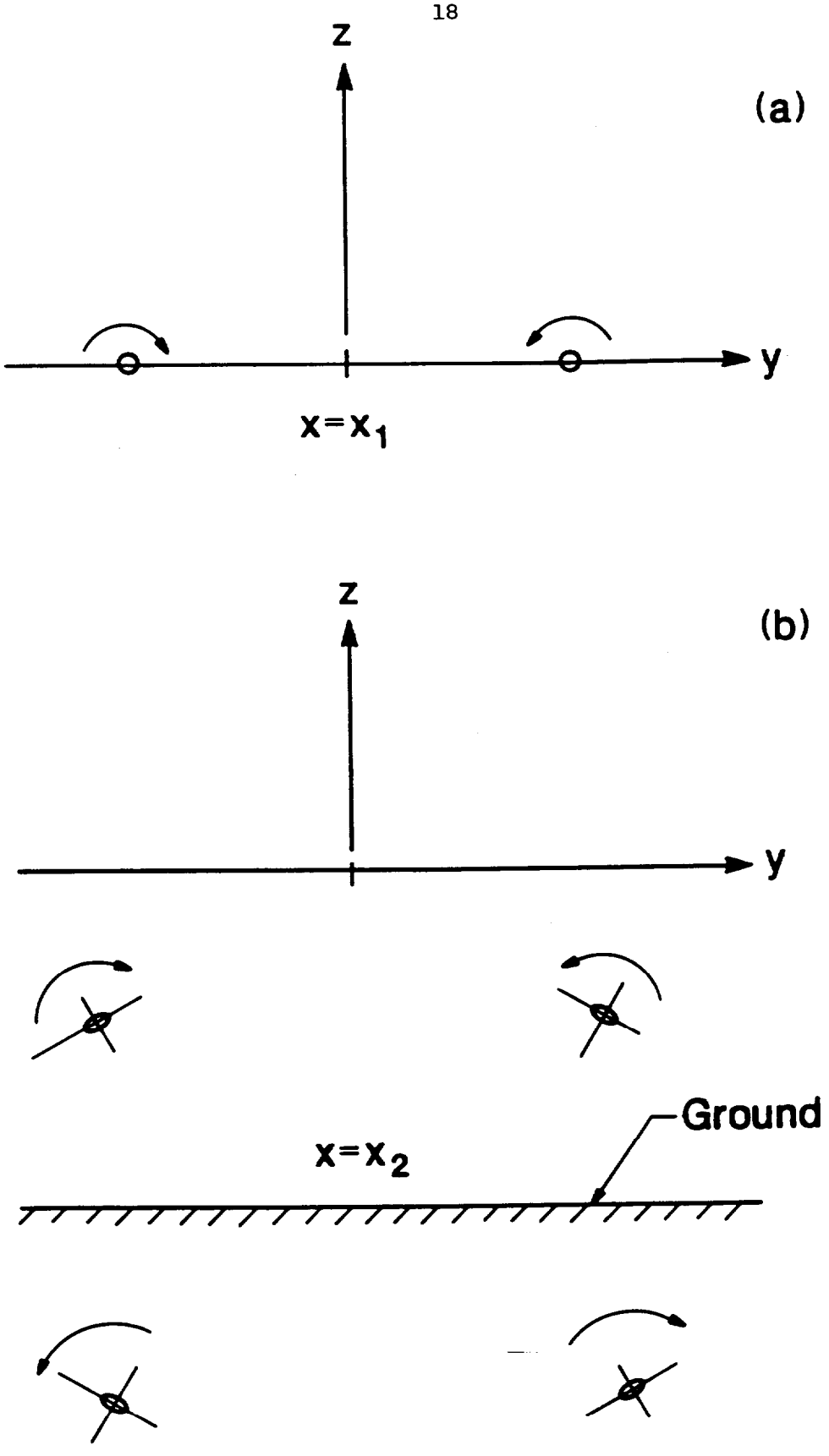

Figure 9. Fluid motion induced by vortices is indicated by direction of arrows. Ground effect is represented by image vortices.

the expression for G. The last two terms account for the image vortices shown in figure 9b generated by the presence of the ground. They induce the swirling motions shown by the arrows which tend to push the clumps of particulate outward as they near the ground.

Discretization

To actually solve the equations defining the problem, it is necessary to discretize the system spatially and integrate the resulting ordinary differential equations in the time like (downwind) direction. There are two crucial issues that must be addressed if the numerical simulation is to accurately approximate the continuous model. First, the velocities and their gradients must be analytically obtained from a discretized form of eqs. (8) and (9). Second, the evolution equations for ω and the coordinate gradients Q, R, S, and T (eqs. (5) and (7)) must be integrated in a mass-conserving scheme.Once these issues are addressed, the remainder of the calculation is similar to other vortex methods.

The key to resolving both issues is the recognition that conservation of mass implies

$$QT-RS = 1. \tag{10}$$

Since the left hand side of equation (10) is also the Jacobian of the transformation between Eulerian and Lagrangian coordinates, it implies that the integral expressing the solution for Ψ in eq. (9) has the same form in Lagrangian coordinates. It can be conceptually discretized in Lagrangian coordinates to $O(h^2)$ accuracy by replacing the integral by a sum of squares of side h and using the value of ω at the center of each square. To the same order accuracy, this can be done with circles of the same area. The crucial point now is to recognize that a small circle of radius r_o in Lagrangian coordinates must be transformed into an ellipse in Eulerian coordinates whose principal semi-axes a, b are given by:

$$\begin{aligned} a^2 &= r_o^2/(\mu + \lambda);\ b^2 = r_o^2/(\mu-\lambda) \\ \mu &= \tfrac{1}{2}(\alpha + \beta) \\ \lambda^2 &= \tfrac{1}{4}\{(\beta-\alpha)^2 + 4\gamma^2\} \\ \alpha &= R^2 + Q^2;\ \beta = S^2 + T^2;\ \gamma = QS + RT \end{aligned} \tag{11}$$

The ellipse is rotated with respect to the Eulerian coordinates by an angle θ obtained from:

$$\tan(2\theta) = 2\gamma/(\alpha-\beta) \tag{12}$$

These expressions exactly preserve area (and hence mass) if eq. (10) is satisfied. The solution for the stream function Ψ for an ellipse containing a uniform prescribed vorticity is well known [12]. Since it is expressed analytically it resolves the first major issue.

To resolve the second point note that eqs. (7), which allow Q,S,R, and T to be advanced in the downwind direction, imply eq. (10) for any set of

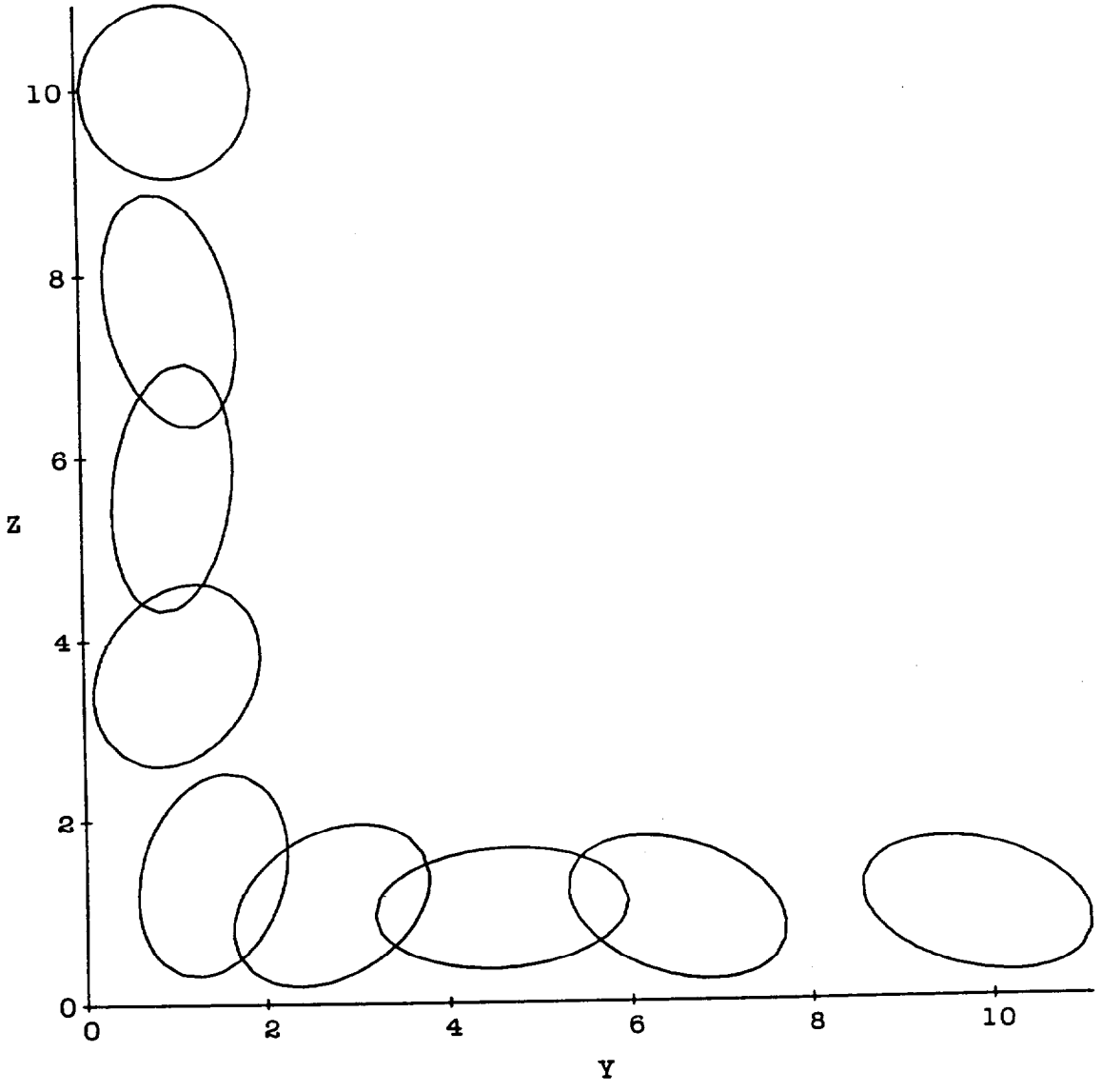

Figure 10. Evolution of right hand member of a vortex pair of constant vorticity as it approaches ground at Z=0. Left hand member is mirror image.

velocity gradients which conserve mass. If now, the velocity gradients are held fixed in time for the duration of a time step δ, then the equations can be analytically integrated. The resulting expressions, which will not be recorded here, exactly preserve eq. (10) for each vortex. Since the analytical results for S and T over the whole time interval δ are available, they can be integrated once more in eq. (5) to obtain an updated value of ω. This value is at least second order accurate in δ. The whole process then is a patchwork of locally exact continuous solutions to the inviscid equations, which, taken together, constitute the discretized problem. The further steps, which involve advecting the ellipses under the influence of the composite velocity field, is common to any vortex method. The evolution of the right hand member of a descending vortex pair is shown in figure 10. The vorticity of each blob is held fixed for illustrative purposes, but the shape and trajectory evolve according to the equations derived above. The shapes are shown at different instants of time. Note that they rotate as well as deform.

The whole approach is similar in spirit to that employed by Ghoniem [13] as a part of his Transport Element Method. Ghoniem retains circular vortices but adds additional ones as needed if the fluid elements become too elongated. Teng [14] has worked with elliptical vortices in simulating constant density viscous flows past a flat plate. However, his ellipses were rigid and non-rotating, which is not locally consistent with the flow kinematics. The present approach attempts to make maximum use of the analytical information available and build it into the computation. It is of necessity more specialized than that of Ghoniem, but hopefully will prove a more faithful representation of the equations it is intended to solve.

FUTURE STUDIES

Preparations are being made for large-scale tests of oilspill burning. This research program is preparing means to make measurements at the large-scale tests that can be compared to existing laboratory data.

ACKNOWLEDGEMENT

Professor R. Dobbins analyzed the aging data to obtain the agglomeration coefficient. This work was supported by the Mineral Management Service of the U.S. Department of the Interior under the supervision of Mr. Edward Tennyson and Mr. John Gregory.

REFERENCES

1. Brown, H.M. and Goodman, R.H., "In Situ Burning of Oil in Ice Leads," Proceedings of the Ninth Annual Arctic and Marine Oilspill Program Technical Seminar, June 10-12, 1986, Edmonton, Alberta, Canada, Environment Canada, Ottawa K1A 0H3, 1986.

2. Smith, K.N. and Diaz, A., "In-Place Burning of Crude oil in Broken Ice: 1985 Testing at OHMSETT," Proceedings of the Eight Annual Arctic Marine

Oilspill Program Technical Seminar, June 18-20, 1985, Edmonton, Alberta, Canada, Environment Canada, Ottawa K1A 0H3, 1985.

3. Buist, I.A. and Twardus, E.M., "Burning Unconfined Oil Slicks: Large Scale Tests and Modelling," Proceedings of the Eight Annual Arctic Marine Oilspill Program Technical Seminar, June 18-20, 1985, Edmonton, Alberta, Canada, Environment Canada, Ottawa K1A 0H3, 1985.

4. Evans, D., Baum, H., McCaffrey, B., Mulholland, G., Harkleroad, M., Manders, W., Combustion of Oil on Water, Report NBSIR 86-3420, National Bureau of Standards, Gaithersburg, MD 20899.

5. Evans, D., Mulholland G., Gross, D., Baum, H., and Saito, K., Environment Effects of Oil Spill Combustion, Report NISTIR 88-3822, National Institute of Standards and Technology, Gaithersburg, MD 20899.

6. Evans, D., Mulholland, G., Gross, D., Baum, H., and Saito, K., Burning, Smoke Production, and Smoke Dispersion from Oil Spill Combustion, NISTIR report in preparation.

7. Jones, A.R., "Scattering Efficiency Factors for Agglomerates of Small Spheres," J. Phys.D: Appl. Phys., **12**, 1661-1672, 1979.

8. Berry, M.V., and Percival, I.C.,"Optics of Fractal Clusters Such as Smoke," Optica Acta, **33**, 577-591, 1986.

9. Cashdollar, K.L., Lee, C.K., and Singer, J.M., "Three-Wavelength Light Transmission Technique to Measure Smoke Particle Size and Concentration," Applied Optics 18, 1763-1769, 1979.

10. Mountain, R.D., Mulholland G.W., and Baum, H., "Simulation of Aerosol Agglomeration in the Free Molecular and Continuum Flow Regimes," J. Colloid and Interface Sci., **114**, 67-81, 1986.

11. Mulholland, G.W., Samson, R.J., Mountain, R.D., and Ernst, M.H., "Cluster Size Distribution for Free Molecular Agglomeration," J. Energy and Fuels, **2**, 481-486, 1988.

12. Lamb, H., Hydrodynamics, Sixth Ed., Dover Pub., New York, p. 230, (1945).

13. Ghoniem, A.F., Heidarinejad, G., and Krishnan, A., "On Mixing, Baroclinicity, and the Effect of Strain in a Chemically-Reacting Shear Layer", AIAA 26th Aerospace Sciences Meeting, Paper AIAA-88-0729, Jan. 11-14, (1988).

14. Teng, Z.H., "Elliptic-Vortex Method for Incompressible Flow at High Reynolds Number", J. Comp. Phys. 46, p.54. (1982).